



Gust Buffeting and Aerodynamic Admittance of Structures with Arbitrary Mode Shapes. I: Enhanced Equivalent Spectrum Technique

Giovanni Solari, M.ASCE¹; and Patricia Martín²

Abstract: The loading and response of structures due to gust buffeting is a dominant topic of wind engineering. One of its crucial aspects is the shape of vibration modes. Although numeric solutions are available for any mode, conceptual interpretations and closed-form solutions mainly are limited to the case in which the sign of the mode does not change along the structural axis. For modes that change sign, it is difficult, if not impossible, to recognize the physical role of the parameters that govern the problem and judge analysis results in qualitative form. This paper addressed this issue in the framework of quasi-steady theory by clarifying the relationship linking aerodynamic admittance with mode shape, showed that any mode may be brought back to a piecewise ensemble of regular modes with constant sign, and used this concept to obtain a closed-form expression for any aerodynamic admittance. This solution is simple for modes with few changes of sign, but becomes laborious as mode complexity increases. In addition, it provides a partial conceptual interpretation. Both of these limits were overcome in the companion paper, in which the use of proper orthogonal decomposition led to a full conceptual interpretation of aerodynamic admittance and a simple and general closed-form solution. DOI: [10.1061/\(ASCE\)EM.1943-7889.0001872](https://doi.org/10.1061/(ASCE)EM.1943-7889.0001872). This work is made available under the terms of the Creative Commons Attribution 4.0 International license, <https://creativecommons.org/licenses/by/4.0/>.

Author keywords: Aerodynamic admittance; Buffeting; Energy cascade; Mode shape; Wind loading.

Introduction

Modern research on the loading and response of structures due to gust buffeting began in the 1960s (Solari 2019). In a series of papers on the dynamic alongwind response of single-degree-of-freedom (SDOF) systems the deformation of which occurs in the mean wind direction, Davenport (1961, 1964, 1967) expressed the mean value of the maximum displacement, called maximum displacement for the sake of simplicity, as the product of the mean static displacement and a nondimensional quantity referred to as gust response factor (GRF). Exploiting structural linearity, Davenport also provided a novel definition of equivalent static force (ESF), namely the force that when statically applied on a structure causes the maximum displacement, as the product of the mean static force and the GRF. Davenport merged rigorous and elegant formulations with physical and engineering interpretations.

Davenport (1962a, b) studied the alongwind, crosswind, and torsional response of monodimensional structures, including the contribution of higher modes by modal analysis. These papers retained Davenport's trademark rigorous and elegant formulation. However, the physical and engineering interpretations were weaker, and were overwhelmed by analytical aspects due to modes that change sign.

The studies carried out in the 1970s followed three distinct pathways. Vellozzi and Cohen (1968), Vickery (1970), and Simiu (1976, 1980) perfected Davenport's original method on SDOF systems with reference to wind and aerodynamic modeling. ESDU (1976) and ECCS (1978) recognized the role of higher modes in the quasi-static part of wind load effects other than displacement, especially the bending moment and shear force; accordingly, they applied the influence function technique, separated the maximum values of the quasi-static and resonant response, and combined them by the square root of the sum of squares invoking statistical independence. Simiu and Lozier (1975) and Solari (1981) implemented the first computer programs to consider the contribution of higher modes by modal analysis.

Solari (1982, 1983) derived the first closed-form solution (CFS) of the alongwind response, taking into account the sole first mode. Continuing this research, Solari (1988) introduced the equivalent wind spectrum technique (EWST), a method by which the partially correlated wind field is schematized as an equivalent field perfectly coherent in space. This enabled Solari to evaluate the wind loading, as well as the seismic loading, by the response spectrum technique (Solari 1989), and to provide a generalized definition of GRF (Solari 1990). In addition, EWST led to an advanced CFS of the alongwind response (Solari 1993a, b), which is a reference for standards and codes (Solari and Kareem 1998; Tamura et al. 2005; Kwon and Kareem 2013).

In the spirit pioneered by ESDU (1976) and ECCS (1978), most of the research in the 1990s derived from the observation that the ESF conceived by Davenport produced correct estimates of displacements but might lead to rough evaluations of different load effects. Gerstoft and Davenport (1986) and Davenport and Sparling (1992) developed the patch loading method through which the quasi-static behavior of guyed masts is determined by the influence function technique, whereas the resonant response is evaluated by modal analysis. Kasperski (1992) proposed the load-response correlation method by which the quasi-static ESF is defined as the

¹Professor, Dept. of Civil, Chemical and Environmental Engineering (DICCA), Polytechnic School, Univ. of Genova, Via Montallegro, 1, Genova 16145, Italy (corresponding author). ORCID: <https://orcid.org/0000-0002-2376-4498>. Email: giovanni.solari@unige.it

²Associate Professor, Dept. of Structures, Technological, Univ. of Havana, José Antonio Echeverría (CUJAE), Havana 19390, Cuba.

Note. This manuscript was submitted on February 11, 2020; approved on August 3, 2020; published online on November 11, 2020. Discussion period open until April 11, 2021; separate discussions must be submitted for individual papers. This paper is part of the *Journal of Engineering Mechanics*, © ASCE, ISSN 0733-9399.

most probable load pattern for each specified wind load effect. Holmes (1994, 1996) used these concepts to derive a CFS of the maximum displacements, bending moments, and shear forces of free-standing lattice towers. Davenport (1995) applied the influence function technique to structures in which the response is affected by higher modes. Other authors used similar approaches (Zhou and Kareem 2001; Holmes 2002; Sparling and Wegner 2006; Carrasco Luzardo et al. 2012; Calotescu and Solari 2016).

In parallel, Piccardo and Solari (1996, 1998a, 2000) studied the three-dimensional (3D) wind-induced loading and response of slender structures. Alongwind, crosswind, and torsional actions were modeled by quasi-steady theory as a linear combination of the longitudinal, lateral, and vertical turbulence components; crosswind forces and torsional moments caused by vortex shedding were schematized as independent of buffeting actions and summed to them. The alongwind, crosswind, and torsional responses, dealt with as uncoupled and each one depending on the related first mode, were derived in closed form by the generalized equivalent spectrum technique (Piccardo and Solari 1998b), a method that extends EWST from the alongwind to the 3D response and originated the 3D GRF. A simplified CFS of the 3D GRF limited to buffeting actions was proposed by Solari (2018).

Continuing this research, the Genoese wind engineering group proposed a technique based on one non-dimensional quantity referred to as the 3-D gust effect factor that provides the mean maximum value of the most relevant wind load effects and the ESF of cantilever slender vertical structures. This technique was evaluated by Piccardo and Solari (2002) in closed form. Based on this, the methods aiming to determine the ESF was classified into three families, referred to as the gust factor, load combination, and global loading techniques (Repetto and Solari 2004). A numerical generalization of the 3D gust effect factor technique was developed by Pagnini (2016) for any slender structure and element.

A dominant aspect of this research concerns mode shapes and influence functions. In this regard, physical interpretations and CFS mainly are limited to the cases in which their sign does not change along the structural axis. Therefore, they usually are precluded to higher modes and to structures with intermediate constraints—e.g., continuous beams, guyed masts, and chimneys linked to buildings—as well as to RC telecommunication towers surmounted by a steel antenna mast. Similarly, the vertical modes of footbridge and bridge decks supported by cables change their sign, whereas the first horizontal mode retains a constant sign; however, due to deck stiffness in its plane, the dominant response often occurs in the vertical direction.

This aspect is essential even in the computer era. The lack of a CFS prevents the engineering and codification sector from using simple methods, does not allow recognizing the role of key parameters in a clear way, and makes it difficult, if not impossible, to deal with the problem conceptually. This happens because without the sign change, the physical role of turbulence coherence is clear and shared: it reduces the resulting loading and response to a greater extent for higher frequencies and longer structures. The change of sign makes this consideration not applicable, links aerodynamic admittance to mode shapes and influence functions, and projects the problem into a framework so complex that it is treatable only numerically.

The lack of literature on this subject is significant. Davenport (1977) examined the joint acceptance function, thus the aerodynamic admittance, of a broad class of structures; focusing on slender models, Davenport depicted the limit trends as a function of the mode shape, without providing an exhaustive interpretation. Dyrbye and Hansen (1988) resumed the study of joint acceptance, solving the double integral in its expression as a chain of two single

integrals. Hansen and Krenk (1999) evaluated the alongwind response of structures with arbitrary modes based on the two previous solutions, but did not provide a full conceptual interpretation of the differences that occur depending on whether the modes change or do not change their sign. Caracoglia (2014) employed EWST to study slender, tall structures under the influence of noise disturbances; the problem of modes changing sign was solved approximately by modal correlation lengths (i.e., admittances), defined in the mean-square convergence sense.

Most codes (CEN 2005; National Research Council 2010) state that structures with vibration modes that have a variable sign require in-depth assessments, without giving any operational tool. The few codes that provide ESFs for different wind load effects (AIJ 2005; ISO 2009) are limited to vertical cantilever structures, in which the influence functions of bending moments and shear forces do not change sign.

This paper and its companion (Solari and Martín 2020) address this issue by investigating the dependence of aerodynamic admittance on modal shape, based on the hypotheses that the structure is slender and linelike, and quasi-steady theory is applied. In particular, this paper first provides the fundamentals of the enhanced equivalent spectrum technique, a method that extends to any mode shape of the generalized equivalent spectrum (Piccardo and Solari 1998b), limited to regular modes that do not change sign. Then it reports some interpretations of specific modes and a closed-form solution based on the principle that any mode may be brought back to a piecewise ensemble of regular modes with constant sign, using the novel concept of stretched modes. Two examples are given that enhance the applicability of this solution to structures with complex modes. Finally, the most relevant results are summarized and the prospects of this research are discussed.

This paper clarified several analytical aspects and derived a solution which is precise and simple for modes with a few changes of sign. However, the solution becomes laborious as mode complexity increases and offers a partial conceptual interpretation of the relationship linking aerodynamic admittance with the mode shape. Both of these limits were overcome by Solari and Martín (2020), in which the application of proper orthogonal decomposition (POD) leads to a simple closed-form solution of aerodynamic admittance and its physical interpretation.

Fundamentals

This section provides the fundamentals of the gust buffeting and aerodynamic admittance of slender structures with arbitrary modes in the framework of quasi-steady theory and modal analysis. It reviews the generalized equivalent spectrum technique (Piccardo and Solari 1998b) and the hypothesis according to which its use is limited to regular modes that do not change sign. Then, it extends this formulation to arbitrary modes through a new method referred to as the enhanced equivalent spectrum technique.

Wind-Excited Response

Consider a structure whose length l is much greater than the reference size b of its cross section; x, y, z is a local Cartesian system with origin at o (Fig. 1); z coincides with the structural axis, x is aligned with the mean wind direction, and o lies at the height H above ground. Furthermore, X, Y, Z is a global Cartesian system with origin at O ; the X, Y -plane is coplanar with the ground; the Y, Z -plane is coplanar with the y, z -plane; X is parallel to x ; Z is directed upward and passes through o ; and z is rotated ϕ with respect to Z .

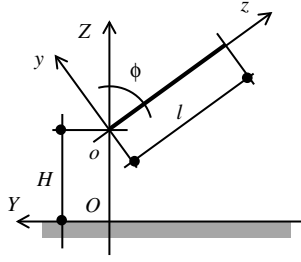


Fig. 1. Structural model and reference systems (X, x entering the page).

The wind loading is schematized as a three-variate (3-V) two-dimensional (2D) stationary Gaussian process, in which the $\alpha = x, y, \theta$ component is given by

$$f_{\alpha}(z, t) = \bar{f}_{\alpha}(z) + f'_{\alpha}(z, t) \quad (1)$$

where $0 \leq z \leq l$; t = time; f_x, f_y , and f_{θ} = alongwind force, crosswind force, and torsional moment per unit length; \bar{f}_{α} = mean value of f_{α} ; and f'_{α} = zero mean fluctuation of f_{α} .

The structure has linear elastic behavior with viscous damping and three uncoupled components of motion, the alongwind displacement x , crosswind displacement y , and torsional rotation θ . Each $\alpha = x, y, \theta$ generalized displacement is a 2D stationary Gaussian process given by

$$\alpha(r, t) = \bar{\alpha}(r) + \alpha'(r, t) \quad (2)$$

where $0 \leq r \leq l$; $\bar{\alpha}$ = mean value of α ; and α' = zero mean fluctuation of α . The maximum value of $|\alpha|$ in period T over which the mean wind velocity is evaluated is given by

$$\bar{\alpha}_{\max}(r) = |\bar{\alpha}(r)| + g_{\alpha}(r)\sigma_{\alpha}(r) \quad (3)$$

$$g_{\alpha}(r) = \sqrt{2 \ln[\Lambda_{\alpha} \nu_{\alpha}(r) T]} + \frac{0.5772}{\sqrt{2 \ln[\Lambda_{\alpha} \nu_{\alpha}(r) T]}} \quad (4)$$

$$s\nu_{\alpha}(r) = \frac{1}{2\pi} \frac{\sigma_{\dot{\alpha}}(r)}{\sigma_{\alpha}(r)} \quad (5)$$

where σ_{α} , g_{α} , and ν_{α} = standard deviation, peak factor, and expected frequency of α , respectively; $\sigma_{\dot{\alpha}}$ = standard deviation of $\dot{\alpha}$; and $\Lambda_{\alpha} = 1$ for $\bar{\alpha} \neq 0$, and $\Lambda_{\alpha} = 2$ for $\bar{\alpha} = 0$ (Piccardo and Solari 1998a, 2000).

Eqs. (3)–(5) are solved by modal analysis, assuming that damping is small and natural frequencies in each direction are well-separated. Unlike in Piccardo and Solari (1998a, 2000) and following Solari (2018), the quasi-static part of $\dot{\alpha}$ is disregarded. Thus

$$\bar{\alpha}(r) = \sum_k \frac{\psi_{\alpha k}(r) \bar{f}_{\alpha k}}{m_{\alpha k} (2\pi n_{\alpha k})^2} \quad (6)$$

$$\sigma_{\alpha}^2(r) = \sum_k \sigma_{B\alpha k}^2(r) + \sum_k \sigma_{R\alpha k}^2(r) \quad (7)$$

$$\sigma_{B\alpha k}^2(r) = \frac{\psi_{\alpha k}^2(r)}{m_{\alpha k}^2 (2\pi n_{\alpha k})^4} \int_0^{\infty} S_{f\alpha k}(n) dn \quad (8)$$

$$\sigma_{R\alpha k}^2(r) = \frac{\psi_{\alpha k}^2(r)}{m_{\alpha k}^2 (2\pi n_{\alpha k})^4} \frac{\pi n_{\alpha k}}{4\xi_{\alpha k}} S_{f\alpha k}(n_{\alpha k}) \quad (9)$$

$$\nu_{\alpha}(r) = \sqrt{\frac{\sum_k n_{\alpha k}^2 \sigma_{R\alpha k}^2(r)}{\sum_k \sigma_{B\alpha k}^2(r) + \sum_k \sigma_{R\alpha k}^2(r)}} \quad (10)$$

where $\sigma_{B\alpha k}$ and $\sigma_{R\alpha k} = k$ th background (quasi-static) and resonant parts of σ_{α} , respectively; n = frequency; $n_{\alpha k}$, $\xi_{\alpha k}$, $m_{\alpha k}$, and $\psi_{\alpha k} = k$ th natural frequency, damping ratio, modal mass, and vibration mode, respectively, in α direction; and $\bar{f}_{\alpha k}$ and $S_{f\alpha k}$ = mean value and power spectral density (PSD), respectively, of k th modal loading in α direction

$$\bar{f}_{\alpha k} = l \int_0^1 \bar{f}_{\alpha}(\zeta) \psi_{\alpha k}(\zeta) d\zeta \quad (11)$$

$$S_{f\alpha k}(n) = l^2 \int_0^1 \int_0^1 S_{f\alpha}(\zeta, \zeta'; n) \psi_{\alpha k}(\zeta) \psi_{\alpha k}(\zeta') d\zeta d\zeta' \quad (12)$$

where $S_{f\alpha}(\zeta, \zeta', n)$ = cross-PSD (CPSD) of $f'_{\alpha}(\zeta, t)$, $f'_{\alpha}(\zeta', t)$; and $\zeta = z/l$ and $\zeta' = z'/l$ = nondimensional coordinates. Expressing the variance of the background displacement as the sum of the modal variances is acceptable only if the contribution of one mode predominates over the other modes. On the other hand, disregard the modal covariances may cause significant errors. This limitation may be overcome by the influence function technique.

Wind Loading Model

Let \bar{u} be the mean wind velocity aligned with X, x (Fig. 1); B_0^2 are the longitudinal (X, x), lateral (Y), and vertical (Z) zero-mean turbulence components, where $u'/\bar{u} \ll 1$, $v'/\bar{u} \ll 1$, and $w'/\bar{u} \ll 1$. They are treated here as uncorrelated (Solari and Tubino 2002). The wind loading model adopted by Piccardo and Solari (1996) is simplified by neglecting vortex shedding (Solari 2018), and identifying the wind loading with the gust buffeting. This approach is appropriate provided that vortex shedding occurs at critical mean wind velocities well below the design wind velocity at which gust buffeting is evaluated. In that case, vortex shedding deserves independent evaluations. Accordingly, \bar{f}_{α} , and f'_{α} are defined as

$$\bar{f}_{\alpha}(\zeta) = \frac{1}{2} \rho \bar{u}^2(\zeta) b \lambda_{\alpha} c_{\alpha u} \quad (13)$$

$$f'_{\alpha}(\zeta, t) = \sum_{\varepsilon} f'_{\alpha \varepsilon}(\zeta, t) = \sum_{\varepsilon} \bar{f}_{\alpha \varepsilon}(\zeta) \varepsilon * (\zeta, t) \quad (14)$$

$$\bar{f}_{\alpha \varepsilon}(\zeta) = \frac{1}{2} \rho \bar{u}^2(\zeta) b \lambda_{\alpha} c_{\alpha \varepsilon} I_{\varepsilon}(\zeta) (1 + \delta_{\varepsilon u}) \quad (15)$$

where ρ = density of air; $\lambda_x = \lambda_y = 1$; $\lambda_{\theta} = b$; and $c_{\alpha \varepsilon} = \alpha$, ε th element of 3×3 aerodynamic matrix the rows of which refer to the loading components $\alpha = x, y, \theta$ and the columns refer to the turbulence components $\varepsilon = u, v, w$

$$[c] = \begin{bmatrix} c_d & (c'_d - c_{\ell}) \cos \phi & (c'_d - c_{\ell}) \sin \phi \\ c_{\ell} & (c_d + c'_{\ell}) \cos \phi & (c_d + c'_{\ell}) \sin \phi \\ c_m & c'_m \cos \phi & c'_m \sin \phi \end{bmatrix} \quad (16)$$

where c_d, c_{ℓ} , and c_m = drag, lift, and torsional moment coefficients; c'_d, c'_{ℓ} , and c'_m = angular prime derivatives; $I_u = \sigma_u/\bar{u}$, $I_v = \sigma_v/\bar{u}$, and $I_w = \sigma_w/\bar{u}$ = turbulence intensities, where σ_u, σ_v , and σ_w = standard deviations of u' , v' , and w' ; $\varepsilon^* = u^* = u'/\sigma_u$, $v^* = v'/\sigma_v$, and $w^* = w'/\sigma_w$; Σ_{ε} = sum of three terms with indices $\varepsilon = u, v, w$; and $\delta_{\varepsilon u}$ = Kronecker's delta. Because f'_{α} is a linear function of ε^* [Eq. (14)], like ε^* , f'_{α} also is a stationary Gaussian process, and its CPSD is

$$S_{f\alpha}(\zeta, \zeta'; n) = \sum_{\varepsilon} \bar{f}_{\alpha\varepsilon}(\zeta) \bar{f}_{\alpha\varepsilon}(\zeta') S_{\varepsilon\varepsilon}^*(\zeta, \zeta'; n) \quad (17)$$

$$S_{\varepsilon\varepsilon}^*(\zeta, \zeta'; n) = \sqrt{S_{\varepsilon}^*(\zeta; n) S_{\varepsilon}^*(\zeta'; n)} \text{Coh}_{\varepsilon\varepsilon}(\zeta, \zeta'; n) \quad (18)$$

where $S_{\varepsilon\varepsilon}^*$, S_{ε}^* , and $\text{Coh}_{\varepsilon\varepsilon}$ = CPSD, PSD, and coherence function of ε^* . Using the turbulence model proposed by Solari and Piccardo (2001)

$$S_{\varepsilon}^*(\zeta; n) = \frac{d_{\varepsilon} L_{\varepsilon}(\zeta) / \bar{u}(\zeta)}{[1 + 1.5 n d_{\varepsilon} L_{\varepsilon}(\zeta) / \bar{u}(\zeta)]^{5/3}} \quad (19)$$

$$\text{Coh}_{\varepsilon\varepsilon}(\zeta, \zeta'; n) = \exp\left\{-\frac{2 n c_{\varepsilon} l |\zeta - \zeta'|}{\bar{u}(\zeta) + \bar{u}(\zeta')}\right\} \quad (20)$$

where $d_u = 6.868$; $d_v = d_w = 9.434$; L_{ε} = integral length scale of ε turbulence component in x -direction; and c_{ε} = exponential decay coefficient of ε along z . Eq. (19) is used in the applications, but may be replaced by any other PSD. Eq. (20) is instead functional to the following developments, but neglects the imaginary part of the CPSD (ESDU 1991), as is typical of all the literature about gust buffeting.

The preceding formulation involves the indices α and ε with the aim of providing the alongwind, crosswind, and torsional actions due to the three turbulence components. If the analysis includes only the alongwind force due to longitudinal turbulence, the indices $\alpha = y, z$, and $\varepsilon = v, w$ disappear, whereas the indices $\alpha = x$ and $\varepsilon = u$ can be omitted, making the treatment easier.

Generalized Equivalent Spectrum Technique

Consider the PSD of the k th modal wind loading in the α direction. Substituting Eqs. (17) and (18) into Eq. (12), it follows that

$$S_{f\alpha k}(n) = l^2 \sum_{\varepsilon} \bar{f}_{\alpha\varepsilon}^2(\bar{\zeta}_{\alpha k}) S_{\varepsilon}^*(\bar{\zeta}_{\alpha k}; n) \times \int_0^1 \int_0^1 \text{Coh}_{\varepsilon\varepsilon}(\zeta, \zeta'; n) \psi_{\alpha k}(\zeta) \psi_{\alpha k}(\zeta') d\zeta d\zeta' \quad (21)$$

where $\bar{\zeta}_{\alpha k}$ is a suitable value of ζ (Solari 2018). In the case of horizontal structures (Fig. 1, $\phi = \pi/2$), the terms evaluated in $\bar{\zeta}_{\alpha k}$ are independent of ζ , and Eq. (21) is rigorous.

The generalized equivalent spectrum technique replaces the actual multivariate turbulent field with an equivalent univariate process, leading to a PSD of the modal wind loading [the first loading in Piccardo and Solari (1998b)] that best approximates the actual PSD. This consists of assuming $\text{Coh}_{\varepsilon\varepsilon} = 1$ and replacing S_{ε}^* with the PSD of the reduced equivalent turbulence

$$S_{\varepsilon, eq}^*(n) = S_{\varepsilon}^*(\bar{\zeta}_{\alpha k}; n) \chi_{\alpha k \varepsilon}(n) \quad (22)$$

Accordingly, Eq. (21) becomes

$$S_{f\alpha k}(n) = l^2 F_{\alpha k}^2 \sum_{\varepsilon} \bar{f}_{\alpha\varepsilon}^2(\bar{\zeta}_{\alpha k}) S_{\varepsilon}^*(\bar{\zeta}_{\alpha k}; n) \chi_{\alpha k \varepsilon}(n) \quad (23)$$

where $F_{\alpha k}$ = participation coefficient; and $\chi_{\alpha k \varepsilon}$ is a frequency filter that plays the role of an aerodynamic admittance. By virtue of Eq. (20)

$$F_{\alpha k} = B_0\{\psi_{\alpha k}\} = \int_0^1 \psi_{\alpha k}(\zeta) d\zeta \quad (24)$$

$$\chi_{\alpha k \varepsilon}(n) = C_0\{\psi_{\alpha k}; \kappa_{\alpha k \varepsilon}(n)\} = \frac{J\{\psi_{\alpha k}; \kappa_{\alpha k \varepsilon}(n)\}}{B_0^2\{\psi_{\alpha k}\}} \quad (25)$$

where J = joint acceptance function; and $\kappa_{\alpha k \varepsilon}$ = reduced frequency

$$J\{\psi_{\alpha k}; \kappa_{\alpha k \varepsilon}(n)\} = \int_0^1 \int_0^1 \exp\{-\kappa_{\alpha k \varepsilon}(n) |\zeta - \zeta'|\} \psi_{\alpha k}(\zeta) \psi_{\alpha k}(\zeta') d\zeta d\zeta' \quad (26)$$

$$\kappa_{\alpha k \varepsilon}(n) = \frac{n c_{\varepsilon} l}{\bar{u}(\bar{\zeta}_{\alpha k})} \quad (27)$$

The aerodynamic admittance coincides with the joint acceptance unless the constant B_0^2 is obtained from the conceptualization of the structure as slender linelike in the framework of quasi-steady theory.

The operator $C_0\{h; \eta\}$ and the aerodynamic admittance $\chi_{\alpha k \varepsilon}$ have the following properties:

1. For $h(\zeta) = 1$, $B_0 = 1$ whereas C_0 is given by (Vellozzi and Cohen 1968):

$$C_0\{1; \eta\} = C \left\{ \frac{\eta}{2} \right\} \quad (28)$$

where C is an operator defined as

$$C\{\omega\} = \frac{1}{\omega} - \frac{1}{2\omega^2} (1 - e^{-2\omega}) \quad \text{for } \omega > 0; C\{0\} = 1 \quad (29)$$

2. For η equal to zero, $C_0\{h; 0\} = 1$;
3. For η tending to infinite, the tail of C_0 is given by (Davenport 1977)

$$C_0\{h; \eta\} = \frac{1}{k\eta}; \quad k = \frac{1}{2} \frac{B_0^2\{h\}}{\int_0^1 h^2(\zeta) d\zeta} \leq \frac{1}{2} \quad (30)$$

where k = equivalent correlation factor, where $k = 1/2$ for $h(\zeta) = 1$; and

4. For $\eta = 0$, C_0 has horizontal tangent and monotonically decreases as η increases.

In the class of structures with regular modes that do not change sign, C_0 can be approximated with excellent precision as (Piccardo and Solari 1998b)

$$C_0\{h; \eta\} = C\{k\eta\} \quad (31)$$

Piccardo and Solari (1998b) evaluated k by an empirical approach that provided results almost coincident with the values furnished by Eq. (30).

Enhanced Equivalent Spectrum Technique

The generalized equivalent spectrum technique provides a robust and simplified framework to determine the wind loading and response of slender structures with modes that have constant sign. To extend this formulation to arbitrary modes, the enhanced equivalent spectrum technique herein is formulated. It retains the definition of the PSD of the modal force given by Eq. (23), but replaces Eqs. (24) and (25) with the following expressions:

$$F_{\alpha k} = B_*\{\psi_{\alpha k}\} = \int_0^1 |\psi_{\alpha k}(\zeta)| d\zeta \quad (32)$$

$$\chi_{\alpha k \varepsilon}(n) = C_*\{\psi_{\alpha k}; \kappa_{\alpha k \varepsilon}(n)\} = \frac{J\{\psi_{\alpha k}; \kappa_{\alpha k \varepsilon}(n)\}}{B_*^2\{\psi_{\alpha k}\}} \quad (33)$$

Unlike B_0 [Eq. (24)], B_* [Eq. (32)] involves the presence of $|\psi_{\alpha k}|$ instead of $\psi_{\alpha k}$ and is called the generalized participation coefficient. The advantage of this change is apparent with regard to structures with skew-symmetric modes with respect to $\zeta = 1/2$: the modulus prevents the denominator of Eq. (33) from being null and

Eq. (23) from being undetermined. Because the new formulation identifies itself with the formulation related to modes that do not change sign, namely $B_* = B_0$ and $C_* = C_0$, the generalized equivalent spectrum technique may be regarded as a particular case of the enhanced equivalent wind spectrum technique. The definition of $\tilde{\chi}_{\alpha k \varepsilon}$ in inclined or vertical structures with complex modes calls for further study.

The operator $C_*\{h; \eta\}$ and the aerodynamic admittance $\chi_{\alpha k \varepsilon}$ have the following properties:

1. For $\psi_{\alpha k}(\zeta) = 1$, $B_* = B_0 = 1$ whereas $C_* = C_0$ is given by Eqs. (28) and (29);
2. For $n = 0$

$$\chi_{\alpha k \varepsilon}(0) = \frac{B_0^2 \{\psi_{\alpha k}\}}{B_*^2 \{\psi_{\alpha k}\}} \leq 1 \quad (34)$$

where $\chi_{\alpha k \varepsilon}(0) = 1$ for vibration modes with constant sign;

3. For $n = 0$, $\chi_{\alpha k \varepsilon}$ has horizontal tangent; however, unlike C_0 , the monotonic decrease of $\chi_{\alpha k \varepsilon} = C_*$ as η increases no longer is guaranteed for modes that change sign; and
4. For n tending to infinity, the tail of $\chi_{\alpha k \varepsilon}$ is given by (Davenport 1977)

$$\chi_{\alpha k \varepsilon}(n) = \frac{1}{k_{\alpha k}^* \kappa_{\alpha k \varepsilon}(n)}; \quad k_{\alpha k}^* = \frac{1}{2} \frac{B_0^2 \{\psi_{\alpha k}\}}{\int_0^1 \psi_{\alpha k}^2(\zeta) d\zeta} \leq \frac{1}{2} \quad (35)$$

where $k_{\alpha k}^* = 1/2$ for $\psi_{\alpha k}(\zeta) = 1$.

Fig. 2 shows the CFS of Eqs. (32) and (33) given by MATLAB version 2019a software for 17 mode shapes $\psi_{\alpha k}$; it also provides $\chi_0 = \chi_{\alpha k \varepsilon}(0)$ [Eq. (34)], the $\kappa_m = \kappa_{\alpha k \varepsilon}$ value for which $\chi_{\alpha k \varepsilon}$ has a relative maximum, the relative maximum χ_{\max} of $\chi_{\alpha k \varepsilon}$, and $k^* = k_{\alpha k}^*$ [Eq. (35)]. Modes are classified into three families (Davenport 1977), Type A, B, and C modes.

Type A modes do not change sign. For Modes 1–5, $\chi_0 = 1$ and $\chi_{\alpha k \varepsilon}$ monotonically decreases as n , κ increases following the trend of Eq. (35) [Fig. 3(a)]. For $\chi_{\alpha k \varepsilon} = C_* = C_0$, Eq. (31) provides a CFS of aerodynamic admittance where $k = k^*$.

Type B modes are skew-symmetric with respect to the structure midpoint, and, more generally, all modes for which $B_0 = 0$ [Eq. (24)]. For Modes 6–12, $\chi_0 = 0$, and $\chi_{\alpha k \varepsilon}$ initially increases as n , κ increases, reaches the maximum χ_{\max} for $\kappa = \kappa_m$, then decreases with the trend of Eq. (35) [Fig. 3(b)].

Type C modes have intermediate shapes and change sign one or more times with or without a regular pattern. For Modes 13–17, $\chi_{\alpha k \varepsilon}$ is intermediate between those associated with Type A and B modes [Fig. 3(c)]. χ_0 [Eq. (34)] provides a measure of how much a Type C mode approaches a Type A ($\chi_0 = 1$) or B ($\chi_0 = 0$) mode.

In other words, as noted by Hansen and Krenk (1999), Type A, B, and C modes give rise to different trends of $\chi_{\alpha k \varepsilon}$ in the low and medium range of $\kappa_{\alpha k \varepsilon}$; on the other hand, as shown by Eq. (35) and Fig. 3(d), in the high-frequency range, all the $\chi_{\alpha k \varepsilon}$ diagrams have the same slope when drawn as a function of the logarithm of $\kappa_{\alpha k \varepsilon}$.

In terms of the aerodynamic admittance growth when the reduced frequency increases, a preliminary but partial interpretation is provided by energy cascade with regard to two elementary structural schemes: a simply supported monospan beam and a simply supported double-span beam. The former has a Type A sinusoidal Mode 2 and the highly coherent large eddies in the low-frequency range cause the maximum displacement. The latter has a Type B sinusoidal Mode 6 in which large eddies cause a self-balanced condition that nullifies displacement. Therefore, it is reasonable that the maximum displacement in a span is attained when eddies acting on that span have a diameter d (proportional to \bar{u}/n) comparable with the span length. This interpretation, however, does not clarify

the issue of the wind loading on the contiguous span, in which the eddy phase shift plays a key role: if eddies are in phase, displacement is nullified; if eddies act counterphase, they cause the maximum displacement. Unfortunately, energy cascade depicts turbulence in a single point, without considering the phase shift of eddies in different points. This issue was studied by Solari and Martín (2020).

Furthermore, neglect the quasi-steady theory, even in structures with Type A modes may involve aerodynamic admittances greater than unity (Davenport 1961, 1964) due to eddy separation. Several studies debated this issue with regard to bridge deck sections (Diana et al. 2001; Hatanaka and Tanaka 2002; Han et al. 2010). In these cases, however, analyses call for experimental or CFD simulations based on a wide range of methods that often lead to different results, thereby introducing other sources of uncertainties. Furthermore, making recourse to experimental or CFD simulations calls for fixing the structural shape, limiting the generality of the solutions. From this point of view, studying aerodynamic admittance in the framework of quasi-steady theory aims to provide solutions, which at present are not available in literature, that may represent a general starting point for research which disregard quasi-steady theory.

Interpretations and Solutions

Based on the enhanced equivalent spectrum technique, this section provides some interpretations that clarify the trend of aerodynamic admittance and a solution that simplifies its evaluation.

Class of Symmetric and Skew-Symmetric Modes

Consider the modal shape

$$\psi_{\alpha k}(\zeta) = \bar{\psi}_{\alpha k}(\zeta) \quad \text{for } \zeta \in [0, 1/2] \quad (36a)$$

$$\psi_{\alpha k}(\zeta) = s \bar{\psi}_{\alpha k}(1 - \zeta) \quad \text{for } \zeta \in (1/2, 1] \quad (36b)$$

where $\bar{\psi}_{\alpha k}$ does not change sign for $\zeta \in [0, 1/2]$; $s = 1$ and $s = -1$ correspond respectively to symmetric modes (Type A Modes 1, 2, and 3 in Fig. 2) and skew-symmetric modes (Type B Modes 6, 7, 8, and 9 in Fig. 2) with regard to $\zeta = 1/2$ [Fig. 4(a)].

The stretched mode $\widehat{\psi}_{\alpha k}(\zeta) = \bar{\psi}_{\alpha k}(\zeta/2)$ corresponds to stretching $\bar{\psi}_{\alpha k}$ [Fig. 4(b)]. Therefore, $\widehat{\psi}_{\alpha k}$ does not change its sign for $\zeta \in [0, 1]$ and belongs to Type A modes. For example, Modes 2 and 4 are the stretched counterparts of half the Modes 6 and 7, respectively.

Substituting Eq. (36) into Eqs. (32) and (33), these latter become

$$F_{\alpha k} = B_0 \left\{ \widehat{\psi}_{\alpha k} \right\} \quad (37)$$

$$\chi_{\alpha k \varepsilon}(n) = \frac{1}{2} C_0 \left\{ \widehat{\psi}_{\alpha k}; \frac{\kappa_{\alpha k \varepsilon}(n)}{2} \right\} + \frac{s}{2} D_0^2 \left\{ \widehat{\psi}_{\alpha k}; \frac{\kappa_{\alpha k \varepsilon}(n)}{2} \right\} \quad (38)$$

where D_0 is an operator defined as

$$D_0 \left\{ \widehat{h}; \eta \right\} = \frac{\int_0^1 \exp\{-\eta \zeta\} \widehat{h}(\zeta) d\zeta}{B_0 \left\{ \widehat{h} \right\}} \quad (39)$$

The first term on the right-hand side of Eq. (38) provides the contribution to $\chi_{\alpha k \varepsilon}$ of the on-diagonal terms in the shaded areas of the integration domain in Fig. 4(c). The second term gives the contribution to $\chi_{\alpha k \varepsilon}$ of the off-diagonal terms in the unshaded areas.

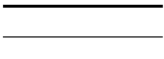


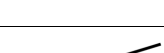
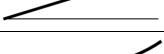

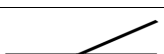
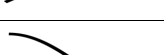
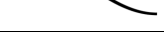
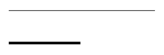
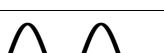
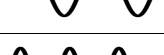

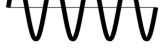
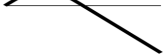

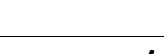
Type	No.	$\psi_{\alpha k}(\zeta)$ for $\zeta \in [0,1]$	$F_{\alpha k}$	$\chi_{\alpha k \varepsilon} = C_*$	χ_0	κ_m	χ_{max}	k^*
A	1	 1	1	$\frac{2}{\kappa} - \frac{2}{\kappa^2}(1 - e^{-\kappa})$	1	0	1	$\frac{1}{2}$
	2	 $\sin(\pi\zeta)$	$\frac{2}{\pi}$	$\frac{\pi^2}{4} \cdot \frac{2\pi^2 + \pi^2\kappa + \kappa^3 + 2\pi^2 e^{-\kappa}}{(\pi^2 + \kappa^2)^2}$	1	0	1	$\frac{4}{\pi^2}$
	3	 $\frac{1}{2}[1 - \cos(2\pi\zeta)]$	$\frac{1}{2}$	$4 \cdot \frac{-32\pi^4 + 32\pi^4\kappa + 20\pi^2\kappa^3 + 3\kappa^5 + 32\pi^4 e^{-\kappa}}{4(4\pi^2\kappa + \kappa^3)^2}$	1	0	1	$\frac{1}{3}$
	4	 ζ	$\frac{1}{2}$	$4 \cdot \frac{6 + \kappa^2(-3 + 2\kappa) - 6(1 + \kappa)e^{-\kappa}}{3\kappa^4}$	1	0	1	$\frac{3}{8}$
	5	 ζ^2	$\frac{1}{3}$	$9 \cdot \frac{-120 + \kappa^3[20 + 3\kappa(-5 + 2\kappa)] + 60[2 + \kappa(2 + \kappa)]e^{-\kappa}}{15\kappa^6}$	1	0	1	$\frac{5}{18}$
B	6	 $\sin(2\pi\zeta)$	$\frac{2}{\pi}$	$\frac{\pi^2}{4} \cdot \frac{8\pi^2 + 4\pi^2\kappa + \kappa^3 - 8\pi^2 e^{-\kappa}}{(4\pi^2 + \kappa^2)^2}$	0	4.22	0.240	$\frac{4}{\pi^2}$
	7	 $2\zeta - 1$	$\frac{1}{2}$	$4 \cdot \frac{2[12 + (\kappa - 3)\kappa^2] - 6(2 + \kappa)^2 e^{-\kappa}}{3\kappa^4}$	0	3.40	0.273	$\frac{3}{8}$
	8	 $\cos(\pi\zeta)$	$\frac{2}{\pi}$	$\frac{\pi^2}{4} \cdot \frac{\kappa[\pi^2 + (-2 + \kappa)\kappa] - 2\kappa^2 e^{-\kappa}}{(\pi^2 + \kappa^2)^2}$	0	3.48	0.263	$\frac{4}{\pi^2}$
	9	 -1 for $\zeta \in [0, \frac{1}{2}]$ 1 for $\zeta \in [\frac{1}{2}, 1]$	1	$\frac{6 - 2\kappa + 2e^{-\kappa} - 8e^{-\kappa/2}}{\kappa^2}$	0	3.80	0.191	$\frac{1}{2}$
	10	 $\sin(4\pi\zeta)$	$\frac{2}{\pi}$	$\frac{\pi^2}{4} \cdot \frac{16\pi^2(2 + \kappa) + \kappa^3 - 32\pi^2 e^{-\kappa}}{(16\pi^2 + \kappa^2)^2}$	0	10.43	0.107	$\frac{4}{\pi^2}$
	11	 $\sin(6\pi\zeta)$	$\frac{2}{\pi}$	$\frac{\pi^2}{4} \cdot \frac{36\pi^2(2 + \kappa) + \kappa^3 - 72\pi^2 e^{-\kappa}}{(36\pi^2 + \kappa^2)^2}$	0	16.76	0.069	$\frac{4}{\pi^2}$
C	12	 $\sin(8\pi\zeta)$	$\frac{2}{\pi}$	$\frac{\pi^2}{4} \cdot \frac{64\pi^2(2 + \kappa) + \kappa^3 - 128\pi^2 e^{-\kappa}}{(64\pi^2 + \kappa^2)^2}$	0	23.06	0.051	$\frac{4}{\pi^2}$
	13	 $\frac{1}{\pi} \sin(2\pi\zeta)$ for $\zeta \in [0, \frac{1}{2}]$ $-2(\zeta - \frac{1}{2})$ for $\zeta \in [\frac{1}{2}, 1]$	$\frac{1}{\pi^2} + \frac{1}{4}$	$\frac{8\pi^4}{3\kappa^4(4 + \pi^2)^2(\pi\kappa^2 + 4\pi^3)^2} \cdot \{e^{-\kappa}[24\kappa^2(2 + \kappa)\pi^2(\kappa^2 + 4\pi^2)] - 96e^{-\frac{\kappa}{2}}\pi^4[\kappa^2(4 + \kappa) + 4\pi^2(2 + \kappa)] + 3\kappa^7 + 2\kappa^4\pi^2[24 + 6\kappa - 3\kappa^2 + \kappa^3] + 16\kappa^2\pi^4[12 - 3\kappa^2 + \kappa^3] + 32\pi^6[24 - 3\kappa^2 + \kappa^3]\}$	0.179	2.79	0.333	0.321
	14	 $-5.5\zeta^2 + 8\zeta^3 - 1.5\zeta^4$	0.3026	Numerical integration	0.194	2.60	0.274	0.344
	15	 $\sin(3\pi\zeta)$	$\frac{2}{\pi}$	$\frac{\pi^2}{4} \cdot \frac{9\pi^2(2 + \kappa) + \kappa^3 + 18\pi^2 e^{-\kappa}}{(9\pi^2 + \kappa^2)^2}$	$\frac{1}{9}$	7.24	0.148	$\frac{4}{\pi^2}$
	16	 $\sin(5\pi\zeta)$	$\frac{2}{\pi}$	$\frac{\pi^2}{4} \cdot \frac{25\pi^2(2 + \kappa) + \kappa^3 + 50\pi^2 e^{-\kappa}}{(25\pi^2 + \kappa^2)^2}$	$\frac{1}{25}$	13.60	0.084	$\frac{4}{\pi^2}$
	17	 $\sin(7\pi\zeta)$	$\frac{2}{\pi}$	$\frac{\pi^2}{4} \cdot \frac{49\pi^2(2 + \kappa) + \kappa^3 + 98\pi^2 e^{-\kappa}}{(49\pi^2 + \kappa^2)^2}$	$\frac{1}{49}$	19.91	0.059	$\frac{4}{\pi^2}$

Fig. 2. Values and expressions of $F_{\alpha k}$, $\chi_{\alpha k \varepsilon} = C_*$, χ_0 , κ_m , χ_{max} , and k^* for noteworthy mode shapes, where $\kappa = \kappa_{\alpha k \varepsilon}(n)$.

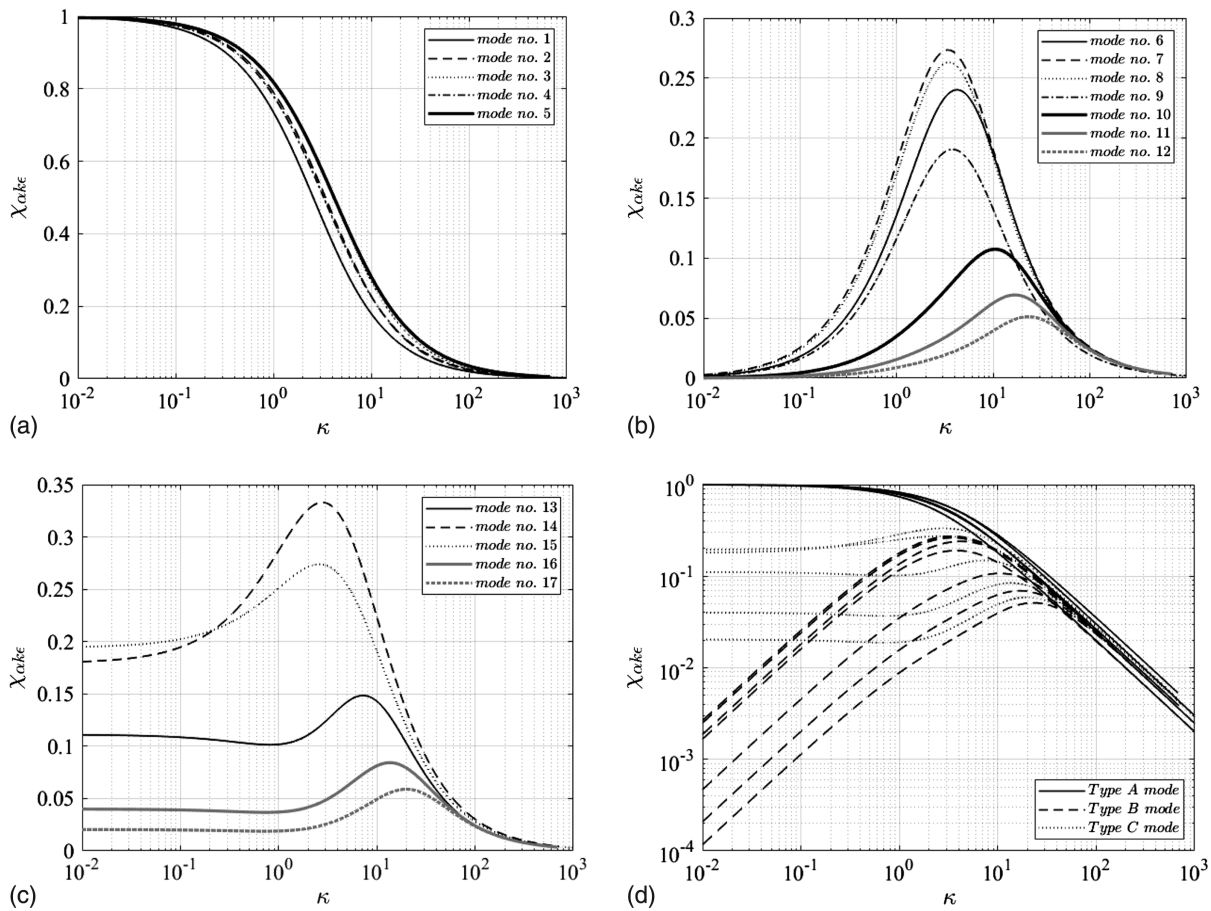


Fig. 3. Diagrams of $\chi_{\alpha k \epsilon}(n)$ as a function of $\kappa = \kappa_{\alpha k \epsilon}(n)$ for different mode shapes $\psi_{\alpha k}$: (a) Type A modes; (b) Type B modes; (c) Type C modes; and (d) all modes on a bilogarithmic scale (solid lines = Type A modes; dashed lines = Type B modes; and dotted lines = Type C modes).

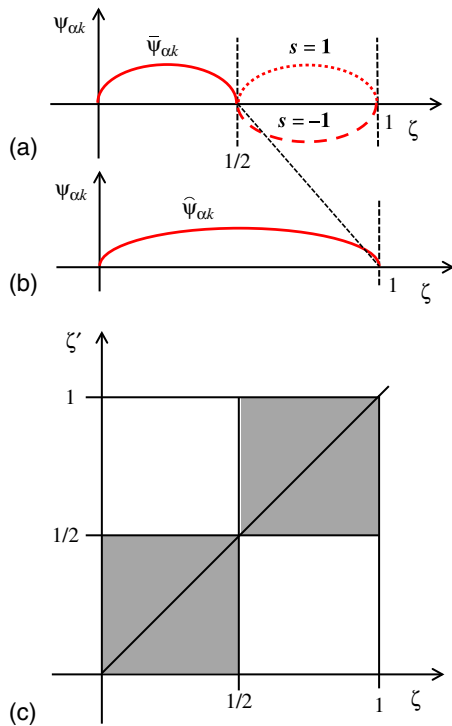


Fig. 4. (a) Symmetric ($s = 1$) and skew-symmetric ($s = -1$) mode shapes $\psi_{\alpha k}$; (b) stretched mode; and (c) integration domain.

The presence of stretched modes with constant sign in Eqs. (38) and (39) makes $B_* = B_0$ and $C_* = C_0$.

The operator $D_0\{\hat{h}; \eta\}$ has the following properties:

1. For $\hat{h}(\zeta) = 1$, $B_0 = 1$ [Eq. (24)], whereas D_0 [Eq. (39)] is given by

$$D_0\{1; \eta\} = D\left\{\frac{\eta}{2}\right\} \quad (40)$$

where D is an operator defined as

$$D\{\omega\} = \frac{1}{2\omega}(1 - e^{-2\omega}) \quad \text{for } \omega \neq 0; \quad D\{0\} = 1 \quad (41)$$

2. For $\eta = 0$, $D_0\{\hat{h}; 0\} = 1$; and
3. For $\eta = 0$, D_0 has horizontal tangent; in addition, it is a monotonic decreasing function of η .

Fig. 5 shows the CFS of Eq. (39) for Type A Modes 1–5, where $\hat{h}(\zeta) = \hat{\psi}_{\alpha k}(\zeta) \geq 0$. Fig. 6 shows the diagrams of D_0 , confirming that, whereas C_0 has an upper tail similar for any mode shape [Eq. (35) and Fig. 3(d)], the upper and lower tails of D_0 depend strictly on the mode. Then, CFS of D_0 and C_0 [Eq. (31)] are not easy to obtain.

The joint properties of D_0 and C_0 clarify two remarkable properties of Eq. (38).

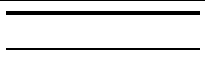


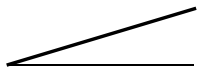
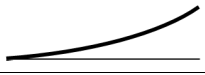
No.	$\hat{h}(\zeta) = \hat{\psi}_{\alpha k}(\zeta)$ for $\zeta \in [0,1]$		D_0
1		1	$\frac{1}{\eta}(1-e^{-\eta})$
2		$\sin(\pi\zeta)$	$\frac{\pi}{2} \frac{\pi(1+e^{-\eta})}{\pi^2 + \eta^2}$
3		$[1 - \cos(2\pi\zeta)]/2$	$2 \cdot \frac{2\pi^2(1+e^{-\eta})}{4\pi^2\eta + \eta^3}$
4		ζ	$2 \cdot \frac{1-(1+\eta)e^{-\eta}}{\eta^2}$
5		ζ^2	$3 \cdot \frac{2-(2+2\eta+\eta^2)e^{-\eta}}{\eta^3}$

Fig. 5. Expressions of D_0 for noteworthy Type A modes, where $\eta = \kappa_{\alpha k \varepsilon}(n)/2$.

For $n = 0$, $\chi_{\alpha k \varepsilon}(0) = (1 + s)/2$. Thus, coherently with Fig. 2, $\chi_{\alpha k \varepsilon}(0) = 1$ for $s = 1$ (symmetric modes), whereas $\chi_{\alpha k \varepsilon}(0) = 0$ for $s = -1$ (skew-symmetric modes).

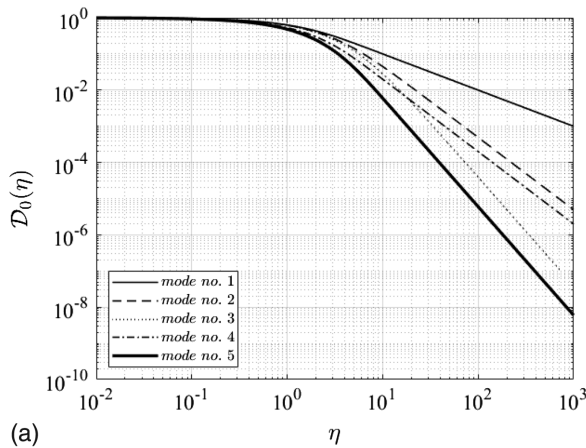
For n tending to infinity, the tail of Eq. (38) is given by Eq. (35), in which the $k_{\alpha k}^*$ value associated with the stretched mode $\hat{\psi}_{\alpha k}$ is given by Fig. 2 for the pertinent Type A mode. Because Eq. (35) is independent of s , the tail of $\chi_{\alpha k \varepsilon}$ is the same independently of whether the mode is symmetric or skew-symmetric. Similarly to Hansen and Krenk (1999), this aspect also may be interpreted partially by energy cascade and the randomness of high-frequency eddies. A better interpretation was given by Solari and Martin (2020).

Class of Mixed Symmetric and Skew-Symmetric Modes

Consider an arbitrary mode $\psi_{\alpha k}(\zeta)$, where $\zeta \in [0, 1]$. It can be expressed as

$$\psi_{\alpha k}(\zeta) = \hat{\psi}_{\alpha k}^{(e)}(\zeta) + \hat{\psi}_{\alpha k}^{(o)}(\zeta) \tag{42}$$

where $\hat{\psi}_{\alpha k}^{(e)}$ and $\hat{\psi}_{\alpha k}^{(o)}$ = symmetric (even) and skew-symmetric (odd) parts of $\psi_{\alpha k}$ with regard to $\zeta = 1/2$, respectively. This representation exists and is unique for any mode. In this section, however, the



use of Eq. (42) is limited to modes $\psi_{\alpha k}^{(e)}$ and $\psi_{\alpha k}^{(o)}$ that do not change sign for $\zeta \in [0, 1/2]$ and $\zeta \in [1/2, 1]$. For example, the algebraic sum of the Type A symmetric Mode 2 and the Type B skew-symmetric Mode 7 provides a Type C intermediate mode.

Substituting Eq. (42) into Eq. (33), the latter becomes

$$\begin{aligned} \chi_{\alpha k \varepsilon}(n) = & \frac{[F_{\alpha k}^{(e)}]^2}{2F_{\alpha k}^2} \left[C_0 \left\{ \hat{\psi}_{\alpha k}^{(e)}; \frac{\kappa_{\alpha k \varepsilon}(n)}{2} \right\} + D_0^2 \left\{ \hat{\psi}_{\alpha k}^{(e)}; \frac{\kappa_{\alpha k \varepsilon}(n)}{2} \right\} \right] \\ & + \frac{[F_{\alpha k}^{(o)}]^2}{2F_{\alpha k}^2} \left[C_0 \left\{ \hat{\psi}_{\alpha k}^{(o)}; \frac{\kappa_{\alpha k \varepsilon}(n)}{2} \right\} - D_0^2 \left\{ \hat{\psi}_{\alpha k}^{(o)}; \frac{\kappa_{\alpha k \varepsilon}(n)}{2} \right\} \right] \end{aligned} \tag{43}$$

where $\hat{\psi}_{\alpha k}^{(e)}(\zeta) = \hat{\psi}_{\alpha k}^{(e)}(\zeta/2)$ and $\hat{\psi}_{\alpha k}^{(o)}(\zeta) = \hat{\psi}_{\alpha k}^{(o)}(\zeta/2)$ = stretched counterparts of half the symmetric and skew-symmetric modes [Figs. 4(a and b)], respectively; $F_{\alpha k}$ is the B_0 operator [Eq. (24)] applied to Eq. (42); and $F_{\alpha k}^{(e)}$ and $F_{\alpha k}^{(o)}$ are defined as

$$F_{\alpha k}^{(e)} = B_* \left\{ \hat{\psi}_{\alpha k}^{(e)} \right\} \quad \text{and} \quad F_{\alpha k}^{(o)} = B_* \left\{ \hat{\psi}_{\alpha k}^{(o)} \right\} \tag{44}$$

The joint properties of D_0 and C_0 clarify two remarkable properties of Eq. (43).

For $n = 0$

$$\chi_{\alpha k \varepsilon}(0) = \frac{[F_{\alpha k}^{(e)}]^2}{F_{\alpha k}^2} \tag{45}$$

For n tending to infinity, the tail of Eq. (43) is provided by the first Eq. (35) in which

$$k_{\alpha k}^* = \frac{1}{\frac{[F_{\alpha k}^{(e)}]^2}{k_{\alpha k}^{(e)} F_{\alpha k}^2} + \frac{[F_{\alpha k}^{(o)}]^2}{k_{\alpha k}^{(o)} F_{\alpha k}^2}} \tag{46}$$

where $k_{\alpha k}^{(e)}$ and $k_{\alpha k}^{(o)} = k_{\alpha k}^*$ values associated with stretched modes $\hat{\psi}_{\alpha k}^{(e)}$ and $\hat{\psi}_{\alpha k}^{(o)}$, respectively, provided by Fig. 2 for the pertinent Type A mode.

For example, considering the sum of the Modes 2 and 7 mentioned above, from Eq. (24), $F_{\alpha k} = 0.835$; from Fig. 2, $F_{\alpha k}^{(e)} = 2/\pi$, $F_{\alpha k}^{(o)} = 1/2$, $k_{\alpha k}^{(e)} = 4/\pi^2$, and $k_{\alpha k}^{(o)} = 3/8$. Therefore, $\chi_{\alpha k \varepsilon}(0) = 0.581$, and $k_{\alpha k}^* = 0.418$.

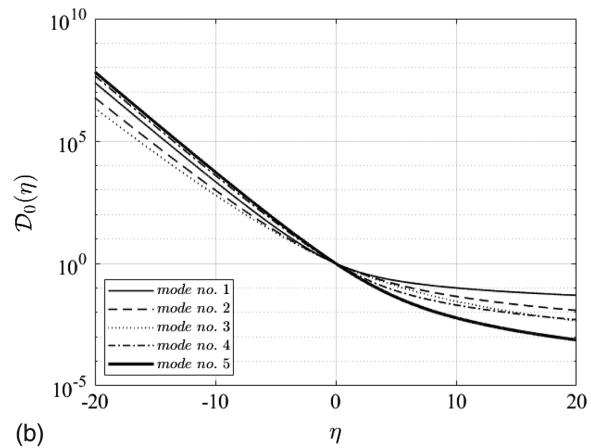


Fig. 6. Diagrams of D_0 as a function of $\eta = \kappa_{\alpha k \varepsilon}(n)/2$ for noteworthy Type A modes: (a) positive η values on logarithmic scale; and (b) negative and positive η values.

Eqs. (45) and (46) give some clarification concerning the shape of the aerodynamic admittance of Type C modes [Fig. 3(c)]. For both $n = 0$ [Eq. (45)] and n tending to infinity [Eq. (46)], $\chi_{\alpha k \varepsilon}$ can be interpreted as a weighted average of the $\chi_{\alpha k \varepsilon}$ functions associated with symmetric Type A and skew-symmetric Type B modes. However, the weights of this average are not constant, but depend on the reduced frequency (Solari and Martín 2020).

Arbitrary Modes

Consider an arbitrary mode $\psi_{\alpha k}(\zeta)$. The $\zeta \in [0, 1]$ domain is separated into a set of subdomains $\zeta \in [\zeta_{i-1}, \zeta_i]$ [Fig. 7(a)], where $i = 1, 2, \dots, N \geq 2$ is the order number, and $\Delta_i = \zeta_i - \zeta_{i-1}$ is the length within which the mode is regular and does not change sign.

Fig. 7(a) depicts the main situations. According to Fig. 7(b), $\widehat{\psi}_{\alpha k}^{(i)}(u)$ is the piecewise mode, where $u = (\zeta - \zeta_{i-1})/\Delta_i \in [0, 1]$, corresponding to stretch $\psi_{\alpha k}(\zeta)$ for $\zeta \in [\zeta_{i-1}, \zeta_i]$; thus, $\widehat{\psi}_{\alpha k}^{(i)}$ does not change sign in $u \in [0, 1]$, and belongs to Type A modes.

Consider Eq. (26) and evaluate the double integral over the domain $\zeta, \zeta' \in [0, 1]$ as the sum of the integrals on the subdomains depicted by Fig. 7(c). Eq. (33) may be rewritten

$$\begin{aligned} \chi_{\alpha k \varepsilon}(n) = & \sum_{i=1}^N \frac{[F_{\alpha k}^{(i)}]^2}{F_{\alpha k}^2} C_0 \left\{ \widehat{\psi}_{\alpha k}^{(i)}; \Delta_i \kappa_{\alpha k \varepsilon}(n) \right\} \\ & + 2 \sum_{i=2}^N \sum_{j=1}^{i-1} \exp\{-\kappa_{\alpha k \varepsilon}(n)(x_{i-1} - x_{j-1})\} \\ & \times \frac{F_{\alpha k}^{(i)} F_{\alpha k}^{(j)}}{F_{\alpha k}^2} D_0 \left\{ \widehat{\psi}_{\alpha k}^{(i)}; \Delta_i \kappa_{\alpha k \varepsilon}(n) \right\} D_0 \left\{ \widehat{\psi}_{\alpha k}^{(j)}; -\Delta_j \kappa_{\alpha k \varepsilon}(n) \right\} \end{aligned} \quad (47)$$

$$F_{\alpha k}^{(i)} = \Delta_i B_0 \left\{ \widehat{\psi}_{\alpha k}^{(i)} \right\} \quad (48)$$

The single sum in Eq. (47) provides the contributions to $\chi_{\alpha k \varepsilon}$ of the on-diagonal terms in the shaded areas of the integration domain

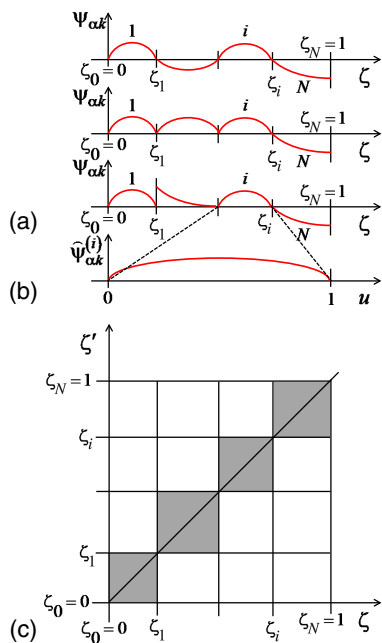


Fig. 7. (a) Three typical arbitrary modes $\psi_{\alpha k}$; (b) stretched mode $\widehat{\psi}_{\alpha k}^{(i)}$ over $u \in [0, 1]$; and (c) integration domain of Eq. (26).

in Fig. 7(c). The double sum provides the contributions to $\chi_{\alpha k \varepsilon}$ of the off-diagonal terms in the unshaded areas.

The joint properties of D_0 and C_0 clarify two remarkable characteristics of Eq. (47).

For $n = 0$

$$\chi_{\alpha k \varepsilon}(0) = \sum_{i=1}^N \frac{[F_{\alpha k}^{(i)}]^2}{F_{\alpha k}^2} + 2 \sum_{i=2}^N \sum_{j=1}^{i-1} \frac{F_{\alpha k}^{(i)} F_{\alpha k}^{(j)}}{F_{\alpha k}^2} \quad (49)$$

Thus, $\chi_{\alpha k \varepsilon}(0) = 1$ for modes with constant sign, and $\chi_{\alpha k \varepsilon}(0) < 1$ for modes that change sign.

For n tending to infinity, the tail of Eq. (47) is provided by the first Eq. (35), in which

$$k_{\alpha k}^* = \frac{1}{\sum_{i=1}^N \frac{[F_{\alpha k}^{(i)}]^2}{F_{\alpha k}^2} \cdot \frac{1}{k_{\alpha k}^{(i)} \Delta_i}} \quad (50)$$

where $k_{\alpha k}^{(i)} = k_{\alpha k}^*$ value associated with stretched mode $\widehat{\psi}_{\alpha k}^{(i)}$ provided by Fig. 2 for pertinent Type A mode, where $k_{\alpha k}^*$ = weighted average of $k_{\alpha k}^{(i)}$ values of its piecewise component Type A modes.

In this framework, aerodynamic admittance can be reconstructed and interpreted as an ensemble of contributions due to the piecewise subdivision of any arbitrary mode into stretched regular modes with constant sign.

Closed-Form Solution

The mathematical and conceptual complexity of this matter makes it difficult to obtain a general CFS of the aerodynamic admittance, which is as simple and precise as that derived by Piccardo and Solari (1998a) for Type A regular modes. Despite this, Eq. (47) can be developed in analytical form.

Consider any Type B or C mode, and divide the structural domain $\zeta \in [0, 1]$ into $N \geq 2$ subdomains within which the piecewise modes are regular and do not change sign (Fig. 7). Thus, the piecewise stretched modes relating to each $i = 1, \dots, N$ subdomain can be modeled by Type A regular modes. Therefore, substituting the corresponding $C_0 = C_*$ (Fig. 2) and D_0 (Fig. 5) operators into Eq. (47), a rigorous $\chi_{\alpha k \varepsilon}$ is obtained if the selected Type A modes rigorously match the actual piecewise stretched modes; an approximate solution is found if they approximate the actual modes or the rigorous expression of C_0 are replaced by Eq. (25). In any case, the reduced frequency κ should be scaled by the appropriate sign and length Δ .

For example, dividing Mode 6 into two piecewise stretched Modes 2 provides a rigorous solution when using the rigorous expressions of C_0 and D_0 ; the solution is approximate when evaluating C_0 with Eq. (25). The application of this method to Mode 14 calls for a preliminary approximation described in the section “Structure 2—Steel Chimney.”

Fig. 8 compares the rigorous expressions of $\chi_{\alpha k \varepsilon}$ given by Eq. (33) for Modes 6, 10, 14, and 15 (solid lines) and Eq. (47) (dashed lines) applied as follows: (1) the actual mode is separated into piecewise stretched regular modes; (2) each of these is approximated by the closest Type A mode; and (3) C_0 is evaluated with Eq. (25), whereas D_0 is obtained from Fig. 5.

Fig. 8 and other diagrams not reported here show that this method provides excellent approximations with errors that do not exceed a few percent for Type B modes and 10% for Type C modes. In addition, it is easy to apply for modes with a few changes of sign. On the other hand, it becomes laborious for more complex modes and does not allow a clear conceptual interpretation of the link

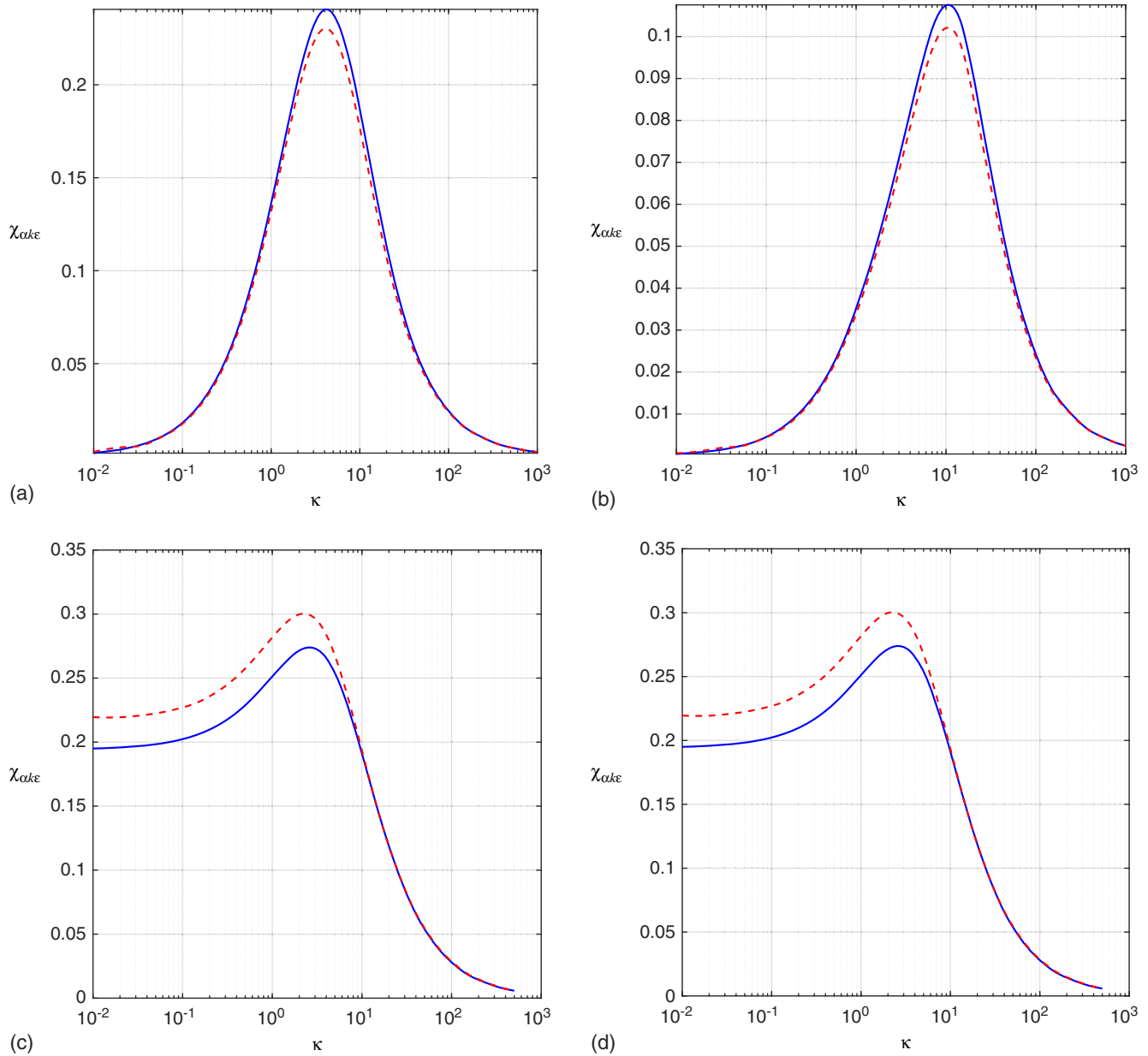


Fig. 8. Rigorous [Eq. (33), solid lines] versus approximate [Eq. (47), dashed lines] diagrams of $\chi_{\alpha k \epsilon}$: (a) Mode 6; (b) Mode 10; (c) Mode 14; and (d) Mode 15.

between aerodynamic admittance and the mode shape. Both of these limitations were overcome by Solari and Martín (2020) through POD.

Applications

To study the efficacy of the aforementioned methods, two structural test cases were analysed: (1) an $l = 90$ -m-long pedestrian steel footbridge [Fig. 9(a), Type B, Mode 6] consisting of a horizontal deck and an arch that sustains the deck by hangers; and (2) an $l = 100$ -m-tall steel chimney constrained to a nearby building at 81 m height [Fig. 9(b), Type C, Mode 14]. The 10-min mean wind speed had a logarithmic profile, and the turbulent field was modeled by Eqs. (18)–(20). Table 1 summarizes the main design parameters. The dynamic response was evaluated by Eqs. (3)–(12),

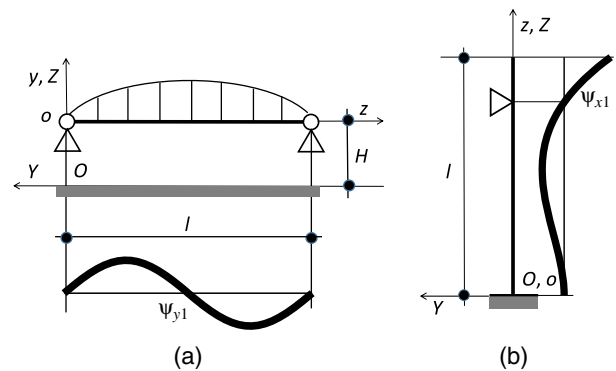


Fig. 9. Structural scheme and modal shape: (a) pedestrian footbridge; and (b) steel chimney.

Table 1. Main parameters of structure test cases

Parameter	Description	Structure 1	Structure 2
ϕ (deg)	Structure inclination (Fig. 1)	$\pi/2$	0
H (m)	Structure height above ground (Fig. 1)	7.1	0
l (m)	Structure length (Fig. 1)	90	100
b (m)	Structure width	5.4	2.8
m (kg/m)	Mass per unit length	170,000	675
α	Displacement direction	y	x
$\psi_{\alpha 1}$	Mode shape	Mode 6	Mode 14
$n_{\alpha 1}$ (Hz)	Fundamental frequency	1.227	0.56
$m_{\alpha 1}$ (kg)	Modal mass	7,650,000	191,893
$\xi_{\alpha 1}$	Damping ratio	0.0036	0.0064
\bar{u} (m/s)	Mean wind speed	18	28
T (s)	Mean wind speed averaging period	600	600
\bar{z} (m)	Reference coordinate	—	50
z_0 (m)	Roughness length	1	0.3
I_u	Longitudinal turbulence intensity	0.3	0.2
I_w	Vertical turbulence intensity	0.075	—
L_u (m)	Longitudinal integral length scale	40	130
L_w (m)	Vertical integral length scale	4	—
c_u	Longitudinal decay coefficient	10	10
c_w	Vertical decay coefficient	6.5	—
c_d	Drag coefficient	—	0.7
c_l	Lift coefficient	−0.35	—
$c_d + c_l'$	Drag plus prime derivative of lift coefficients	6.5	—
$\bar{f}_{\alpha u}$ (N/m)	Quantity defined by Eq. (15) for $\varepsilon = u$	−229.63	384.16
$\bar{f}_{\alpha w}$ (N/m)	Quantity defined by Eq. (15) for $\varepsilon = w$	533.08	—

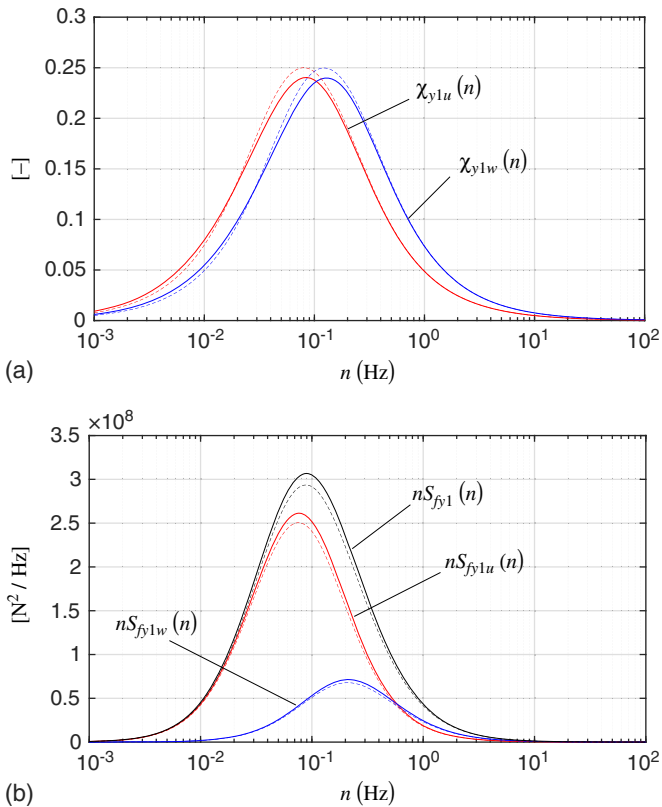


Fig. 10. Pedestrian footbridge: (a) aerodynamic admittances; and (b) PSD of the modal force.

determining aerodynamic admittance by the rigorous Eq. (33) and the CFS of Eq. (47). This solution aimed to furnish simplified and possibly precise evaluations but, even more, to clarify the shape of aerodynamic admittance and its dependence on design parameters.

Table 2. Displacement parameters of Structure 1 for $z = l/4$

Parameter	Equation	Rigorous	Approximate	Error (%)
\bar{y} (m)	(6)	-0.4823×10^{-4}	-0.4823×10^{-4}	—
σ_{By1} (m)	(8)	0.2484×10^{-4}	0.2429×10^{-4}	−2
σ_{Ry1} (m)	(9)	0.1071×10^{-3}	0.1049×10^{-3}	−2
σ_y (m)	(7)	0.1099×10^{-3}	0.1077×10^{-3}	−2
ν_y (Hz)	(10)	1.196	1.195	—
g_y	(4)	3.785	3.785	—
\bar{y}_{\max} (m)	(3)	-0.4642×10^{-3}	-0.4559×10^{-3}	−2

Structure 1—Pedestrian Footbridge

The crosswind fluctuating load in the vertical direction y is due to the longitudinal and vertical turbulence components, u' and w' . Fig. 10 shows the aerodynamic admittances and the PSD of the modal force. Solid lines correspond to the rigorous solution, and dotted lines correspond to the CFS. As is typical of skew-symmetric modes, aerodynamic admittances were null at the zero frequency and their maximum was well below unity. The modal force was due mainly to longitudinal turbulence.

Table 2 lists the main parameters of the vertical displacement for $z = l/4$ due to the first vertical Mode 6. The CFS was applied through Eq. (47) by separating the actual mode into $N = 2$ piecewise half-sine modes that rigorously resembled the original mode, and were $\Delta_1 = \Delta_2 = 1/2$, $F_{yk}^{(1)} = F_{yk}^{(2)} = 1/\pi$, $F_{yk} = 2/\pi$, and $k_{yk}^{(1)} = k_{yk}^{(2)} = 4/\pi^2$.

The CFS provided almost exact results. As is typical of skew-symmetric modes, the background response was small and the resonant response prevailed regardless of structural flexibility.

Structure 2—Steel Chimney

The alongwind fluctuating load is due to the longitudinal turbulence. Fig. 11 shows the aerodynamic admittance and the PSD

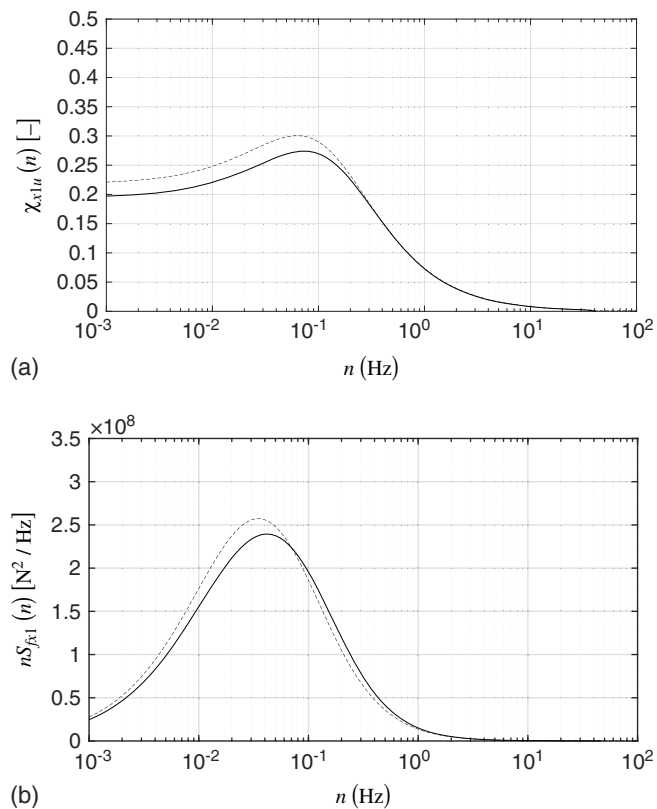


Fig. 11. Steel chimney: (a) aerodynamic admittance; and (b) PSD of the modal force.

Table 3. Displacement parameters of Structure 2 for $z = l$

Parameter	Equation	Rigorous	Approximate	Error (%)
\bar{x} (m)	(6)	-0.00323	-0.00323	—
σ_{Bx1} (m)	(8)	0.00225	0.00235	+4
σ_{Rx1} (m)	(9)	0.00495	0.00495	—
σ_x (m)	(7)	0.00544	0.00548	+1
ν_x (Hz)	(10)	0.510	0.506	-1
g_x	(4)	3.554	3.552	—
\bar{x}_{\max} (m)	(3)	0.0226	0.0227	—

of the modal force. Solid lines correspond to the rigorous solution, dotted lines to the CFS. As is typical of intermediate modes, the aerodynamic admittance was well below unity over the whole frequency range, so it quite uniformly eroded the harmonic content of the modal force.

Table 3 lists the main parameters of the alongwind displacement for $z = l$ due to the first longitudinal Mode 14. The CFS was applied by separating the actual mode in $N = 2$ piecewise modes that resembled the original mode in an approximate way: the $i = 1$ piecewise mode was intermediate between Modes 2 and 3, and the $i = 2$ piecewise mode was intermediate between Modes 4 and 5. The C_0 and D_0 operators in Eq. (47) were evaluated for each piecewise mode as the mean of the related operators, and were $\Delta_1 = 0.81$, $\Delta_2 = 0.19$, $F_{xk}^{(1)} = 0.217$, $F_{xk}^{(2)} = 0.079$, $F_{xk} = 0.296$, and $k_{xk}^{(1)} = 0.369$, $k_{xk}^{(2)} = 0.326$.

Despite the preceding approximations, the CFS gave rise to almost negligible errors.

Conclusions and Prospects

In a series of papers published in the 1960s on the dynamic alongwind response of SDOF systems, Davenport merged rigorous and elegant formulations with physical and engineering interpretations. This was facilitated by the fact that the partial correlation of the oncoming turbulence causes an aerodynamic admittance which, based on energy cascade, decreases with increasing frequency of eddies and with increasing structure size.

The situation is different when structural loading and response involve vibration modes that change sign. This projects the problem into a framework that usually precludes the derivation of simple solutions and makes the problem treatable only numerically. This prevents interpreting the physical, conceptual, and engineering meaning of aerodynamic admittance.

This paper investigated the role of arbitrary mode shapes on the aerodynamic admittance of structures subjected to gust buffeting in the alongwind, crosswind, and torsional directions. Analyses were restricted to slender structures and single modes. The formulation was based on quasi-steady theory and neglected as usual the imaginary part of the turbulence cross-spectrum in order to establish a simple background that may represent the basis for future studies which remove simplifying hypotheses.

The fundamentals of the generalized equivalent spectrum technique were reviewed, stressing its property of being applicable only to structures with a fundamental regular mode that does not change sign. A new method, referred to as the enhanced equivalent spectrum technique, was formulated which is applicable to structures with arbitrary modes and contains the generalized equivalent spectrum technique as a particular case. Special emphasis was given to the dependence of aerodynamic admittance on the mode shape.

Aerodynamic admittance was investigated for a broad class of modes. Based on their trend and on Davenport's intuitions, they are classified into three families, Type A, B, and C modes. Type A modes do not change sign and give rise to classical aerodynamic admittances that decrease as the frequency increases. Type B modes are skew-symmetric with respect to the structure midpoint and give rise to aerodynamic admittances that are null at the zero frequency, increase up to a maximum as frequency increases, then decrease and tending to zero. Type C modes have intermediate shapes and lead to intermediate trends.

That aerodynamic admittance decreases as frequency increases for Type A modes whereas it has a relative maximum for Type B and C modes is a watershed for the physical interpretation of the problem and the formulation of simple solutions.

Based on energy cascade, the maximum load related to modes with constant sign is due to large eddies with a low frequency content, whereas for modes that change sign it is reasonable that the maximum load occurs for eddies the frequency of which corresponds to a diameter with half the wavelength in which the mode has constant sign. However, energy cascade depicts turbulence at a single point, without giving any information about the phase shift of eddies at different points; thus, it does not clarify the role of the load on contiguous half wavelengths, where the mode has opposite sign.

Focusing on simple solutions, this paper dealt with arbitrary modes by dividing the structural domain into subdomains in which piecewise modes are regular and do not change sign. This allowed derivation of a solution based on the application of classical methods to each subdomain. This solution is precise and simple for modes that change sign a limited number of times; on the other hand, it becomes more and more laborious as mode complexity increases.

These limitations were overcome by Solari and Martín (2020) through POD, which leads to physical interpretations from which a simple-closed form solution of aerodynamic admittance derives.

Data Availability Statement

Data, models, or code that support the findings of this study are available from the corresponding author upon reasonable request.

Acknowledgments

The research carried out for this paper by the first author and partly by the second is funded by the European Research Council (ERC) under the European Union's Horizon 2020 research and innovation program (Grant agreement No. 741273) for the Project THUNDERR - Detection, simulation, modelling and loading of thunderstorm outflows to design wind-safer and cost-efficient structures, supported by an Advanced Grant (AdG) 2016. The authors are grateful to Prof. Giuseppe Piccardo, DICCA, University of Genova, and to Prof. Riccardo Brugia, Liceo Cassini, Genova, for the inspiring discussions and unselfish support.

References

- AIJ (Architectural Institute of Japan). 2005. *AIJ Recommendations for loads on buildings*. Tokyo: AIJ.
- Calotescu, P. I., and G. Solari. 2016. "Alongwind load effects on free-standing lattice towers." *J. Wind Eng. Ind. Aerodyn.* 155 (Aug): 182–196. <https://doi.org/10.1016/j.jweia.2016.06.004>.
- Caracoglia, L. 2014. "A stochastic model for examining along-wind loading uncertainty and intervention costs due to wind-induced damage on tall buildings." *Eng. Struct.* 78 (Nov): 121–132. <https://doi.org/10.1016/j.engstruct.2014.07.023>.
- Carrasco Luzardo, A., V. Elena Parnás, and P. Martín Rodríguez. 2012. "Guy tension influence on the structural behavior of a guyed mast." *J. Int. Assoc. Shell Spatial Struct.* 53 (2): 111–116.
- CEN (European Committee for Standardization). 2005. *Eurocode 1: Actions on structures—Part 1-4: Actions in general—Wind actions*. EN 1991-1-4. Brussels, Belgium: CEN.
- Davenport, A. G. 1961. "The application of statistical concepts to the wind loading of structures." *Proc. Inst. Civ. Eng.* 19 (4): 449–472. <https://doi.org/10.1680/iicep.1961.11304>.
- Davenport, A. G. 1962a. "Buffeting of a suspension bridge by storm winds." *J. Struct. Div.* 88 (3): 233–268.
- Davenport, A. G. 1962b. "The response of slender, line-like structures to a gusty wind." *Proc. Inst. Civ. Eng.* 23 (3): 389–408. <https://doi.org/10.1680/iicep.1962.10876>.
- Davenport, A. G. 1964. "The buffeting of large superficial structures by atmospheric turbulence." *Ann. N. Y. Acad. Sci.* 116 (1): 135–160. <https://doi.org/10.1111/j.1749-6632.1964.tb33943.x>.
- Davenport, A. G. 1967. "Gust loading factors." *J. Struct. Div.* 93 (3): 11–34.
- Davenport, A. G. 1977. "The prediction of the response of structures by gusty wind." In *Safety of structures under dynamic loading*, edited by I. Holand, D. Mavlie, G. Moe, and R. Sigbjörnsson, 257–284. Trondheim, Norway: Tapir.
- Davenport, A. G. 1995. "How can we simplify and generalize wind loads." *J. Wind Eng. Ind. Aerodyn.* 54–55 (Feb): 657–669. [https://doi.org/10.1016/0167-6105\(94\)00079-S](https://doi.org/10.1016/0167-6105(94)00079-S).
- Davenport, A. G., and B. F. Sparling. 1992. "Dynamic gust response factors for guyed towers." *J. Wind Eng. Ind. Aerodyn.* 43 (1–3): 2237–2248. [https://doi.org/10.1016/0167-6105\(92\)90662-T](https://doi.org/10.1016/0167-6105(92)90662-T).
- Diana, G., S. Bruni, A. Cigada, and E. Zappa. 2001. "Complex aerodynamic admittance function role in buffeting response of a bridge deck." *J. Wind Eng.* 89 (12–15): 277–280. [https://doi.org/10.1016/S0167-6105\(02\)00321-5](https://doi.org/10.1016/S0167-6105(02)00321-5).
- Dyrbye, C., and S. O. Hansen. 1988. "Calculation of joint acceptance function for line-like structures." *J. Wind Eng. Ind. Aerodyn.* 31 (2–3): 351–353. [https://doi.org/10.1016/0167-6105\(88\)90014-1](https://doi.org/10.1016/0167-6105(88)90014-1).
- ECCS (European Convention for Constructional Steelwork). 1978. *Recommendations for the calculation of wind effects on buildings and structures*. Brussels, Belgium: ECCS.
- ESDU (Engineering Sciences Data Unit). 1976. *The response of flexible structures to atmospheric turbulence*. London: ESDU.
- ESDU (Engineering Sciences Data Unit). 1991. *Characteristics of atmospheric turbulence near the ground. Part III: Variations in space and time for strong winds (neutral atmosphere)*. London: ESDU.
- Gerstoft, P., and A. G. Davenport. 1986. "A simplified method for dynamic analysis of a guyed mast." *J. Wind Eng. Ind. Aerodyn.* 23: 487–499. [https://doi.org/10.1016/0167-6105\(86\)90065-6](https://doi.org/10.1016/0167-6105(86)90065-6).
- Han, Y., Z. Q. Chen, and X. G. Hua. 2010. "New estimation methodology of six complex aerodynamic admittance functions." *Wind Struct.* 13 (3): 293–307. <https://doi.org/10.12989/was.2010.13.3.293>.
- Hansen, S. O., and S. Krenk. 1999. "Dynamic along-wind response of simple structures." *J. Wind Eng. Ind. Aerodyn.* 82 (1–3): 147–171. [https://doi.org/10.1016/S0167-6105\(98\)00215-3](https://doi.org/10.1016/S0167-6105(98)00215-3).
- Hatanaka, A., and H. Tanaka. 2002. "New estimation method of aerodynamic admittance function." *J. Wind Eng. Ind. Aerodyn.* 90 (12–15): 2073–2086. [https://doi.org/10.1016/S0167-6105\(02\)00324-0](https://doi.org/10.1016/S0167-6105(02)00324-0).
- Holmes, J. D. 1994. "Along-wind response of lattice towers: Part I—Derivation of expressions for gust response factors." *Eng. Struct.* 16 (4): 287–292. [https://doi.org/10.1016/0141-0296\(94\)90069-8](https://doi.org/10.1016/0141-0296(94)90069-8).
- Holmes, J. D. 1996. "Along-wind response of lattice towers—III. Effective load distributions." *Eng. Struct.* 18 (7): 489–494. [https://doi.org/10.1016/0141-0296\(95\)00166-2](https://doi.org/10.1016/0141-0296(95)00166-2).
- Holmes, J. D. 2002. "Effective static load distributions in wind engineering." *J. Wind Eng. Ind. Aerodyn.* 90 (2): 91–109. [https://doi.org/10.1016/S0167-6105\(01\)00164-7](https://doi.org/10.1016/S0167-6105(01)00164-7).
- ISO (International Standards Organization). 2009. *Wind actions on structures*. ISO 4354. Geneva, Switzerland: ISO.
- Kasperski, M. 1992. "Extreme wind load distributions for linear and non-linear design." *Eng. Struct.* 14 (1): 27–34. [https://doi.org/10.1016/0141-0296\(92\)90005-B](https://doi.org/10.1016/0141-0296(92)90005-B).
- Kwon, D. K., and A. Kareem. 2013. "Comparative study of major international wind codes and standards for wind effects on tall buildings." *Eng. Struct.* 51 (Jun): 23–35. <https://doi.org/10.1016/j.engstruct.2013.01.008>.
- National Research Council. 2010. *Guide for the assessment of wind actions and effects on structures*. CNR-DT 207/2008. Rome: National Research Council.
- Pagnini, L. C. 2016. "A numerical approach for the evaluation of wind-induced effects on inclined, slender structural elements." *Eur. J. Environ. Civ. Eng.* 21 (7–8): 854–873. <https://doi.org/10.1080/19648189.2016.1164088>.
- Piccardo, G., and G. Solari. 1996. "A refined model for calculating 3-D equivalent static wind forces on structures." *J. Wind Eng. Ind. Aerodyn.* 65 (1–8): 21–30. [https://doi.org/10.1016/S0167-6105\(97\)00019-6](https://doi.org/10.1016/S0167-6105(97)00019-6).
- Piccardo, G., and G. Solari. 1998a. "Closed form prediction of 3-D wind-excited response of slender structures." *J. Wind Eng. Ind. Aerodyn.* 74–76 (Apr): 697–708. [https://doi.org/10.1016/S0167-6105\(98\)00063-4](https://doi.org/10.1016/S0167-6105(98)00063-4).
- Piccardo, G., and G. Solari. 1998b. "Generalized equivalent spectrum technique." *Wind Struct.* 1 (2): 161–174. <https://doi.org/10.12989/was.1998.1.2.161>.
- Piccardo, G., and G. Solari. 2000. "3D wind-excited response of slender structures: Closed-form solution." *J. Struct. Eng.* 126 (8): 936–943. [https://doi.org/10.1061/\(ASCE\)0733-9445\(2000\)126:8\(936\)](https://doi.org/10.1061/(ASCE)0733-9445(2000)126:8(936)).
- Piccardo, G., and G. Solari. 2002. "3-D gust effect factor for slender vertical structures." *Prob. Eng. Mech.* 17 (2): 143–155. [https://doi.org/10.1016/S0266-8920\(01\)00034-0](https://doi.org/10.1016/S0266-8920(01)00034-0).

- Repetto, M. P., and G. Solari. 2004. "Equivalent static wind actions on vertical structures." *J. Wind Eng. Ind. Aerodyn.* 92 (5): 335–357. <https://doi.org/10.1016/j.jweia.2004.01.002>.
- Simiu, E. 1976. "Equivalent static wind loads for tall building design." *J. Struct. Div.* 102 (4): 719–737.
- Simiu, E. 1980. "Revised procedure for estimating along-wind response." *J. Struct. Div.* 106 (1): 1–10.
- Simiu, E., and D. W. Lozier. 1975. *The buffeting of tall structures by strong winds. Building science series*. Washington, DC: Center for Building Technology, National Bureau of Standards.
- Solari, G. 1981. *DAWROS: A computer program for calculating the dynamic along-wind response of structures*. Genova, Italy: Istituto di Scienza delle Costruzioni, Univ. of Genova.
- Solari, G. 1982. "Alongwind response estimation: Closed form solution." *J. Struct. Div.* 108 (1): 225–244.
- Solari, G. 1983. "Analytical estimation of the along-wind response of structures." *J. Wind Eng. Ind. Aerodyn.* 14 (1–3): 467–477. [https://doi.org/10.1016/0167-6105\(83\)90047-8](https://doi.org/10.1016/0167-6105(83)90047-8).
- Solari, G. 1988. "Equivalent wind spectrum technique: Theory and applications." *J. Struct. Eng.* 114 (6): 1303–1323. [https://doi.org/10.1061/\(ASCE\)0733-9445\(1988\)114:6\(1303\)](https://doi.org/10.1061/(ASCE)0733-9445(1988)114:6(1303)).
- Solari, G. 1989. "Wind response spectrum." *J. Eng. Mech.* 115 (9): 2057–2073. [https://doi.org/10.1061/\(ASCE\)0733-9399\(1989\)115:9\(2057\)](https://doi.org/10.1061/(ASCE)0733-9399(1989)115:9(2057)).
- Solari, G. 1990. "A generalized definition of gust factor." *J. Wind Eng. Ind. Aerodyn.* 36 (Part 1): 539–548. [https://doi.org/10.1016/0167-6105\(90\)90336-B](https://doi.org/10.1016/0167-6105(90)90336-B).
- Solari, G. 1993a. "Gust buffeting. I: Peak wind velocity and equivalent pressure." *J. Struct. Eng.* 119 (2): 365–382. [https://doi.org/10.1061/\(ASCE\)0733-9445\(1993\)119:2\(365\)](https://doi.org/10.1061/(ASCE)0733-9445(1993)119:2(365)).
- Solari, G. 1993b. "Gust buffeting. II: Dynamic alongwind response." *J. Struct. Eng.* 119 (2): 383–398. [https://doi.org/10.1061/\(ASCE\)0733-9445\(1993\)119:2\(383\)](https://doi.org/10.1061/(ASCE)0733-9445(1993)119:2(383)).
- Solari, G. 2018. "Gust buffeting of slender structures and structural elements: Simplified formulas for design calculations and code provisions." *J. Struct. Eng.* 144 (2): 04017185. [https://doi.org/10.1061/\(ASCE\)ST.1943-541X.0001949](https://doi.org/10.1061/(ASCE)ST.1943-541X.0001949).
- Solari, G. 2019. *Wind science and engineering: Origins, developments, fundamentals and advancements*. Cham, Switzerland: Springer.
- Solari, G., and A. Kareem. 1998. "On the formulation of ASCE7-95 gust effect factor." *J. Wind Eng. Ind. Aerodyn.* 77–78 (Sep): 673–684. [https://doi.org/10.1016/S0167-6105\(98\)00182-2](https://doi.org/10.1016/S0167-6105(98)00182-2).
- Solari, G., and P. Martín. 2020. "Gust buffeting and aerodynamic admittance of structures with arbitrary mode shapes. II: POD-based interpretation." *J. Eng. Mech.* 147 (1): 04020143. [https://doi.org/10.1061/\(ASCE\)EM.1943-7889.0001873](https://doi.org/10.1061/(ASCE)EM.1943-7889.0001873).
- Solari, G., and G. Piccardo. 2001. "Probabilistic 3-D turbulence modeling for gust buffeting of structures." *Prob. Eng. Mech.* 16 (1): 73–86. [https://doi.org/10.1016/S0266-8920\(00\)00010-2](https://doi.org/10.1016/S0266-8920(00)00010-2).
- Solari, G., and F. Tubino. 2002. "A turbulence model based on principal components." *Prob. Eng. Mech.* 17 (4): 327–335. [https://doi.org/10.1016/S0266-8920\(02\)00016-4](https://doi.org/10.1016/S0266-8920(02)00016-4).
- Sparling, B. F., and L. D. Wegner. 2006. "Comparison of frequency- and time-domain analyses for guyed masts in turbulent winds." *Can. J. Civ. Eng.* 33 (2): 169–182. <https://doi.org/10.1139/l05-101>.
- Tamura, Y., A. Kareem, G. Solari, K. C. S. Kwok, J. D. Holmes, and W. H. Melbourne. 2005. "Aspects of the dynamic wind-induced response of structures and codification." *Wind Struct.* 8 (4): 251–268. <https://doi.org/10.12989/was.2005.8.4.251>.
- Vellozzi, J., and E. Cohen. 1968. "Gust response factors." *J. Struct. Div.* 94 (6): 1295–1313.
- Vickery, B. J. 1970. "On the reliability of gust loading factors." In *Proc., Technical Meeting Concerning Wind Loads on Buildings and Structures*, 93–104. Washington, DC: National Bureau of Standards.
- Zhou, Y., and A. Kareem. 2001. "Gust loading factor: New model." *J. Struct. Eng.* 127 (2): 168–175. [https://doi.org/10.1061/\(ASCE\)0733-9445\(2001\)127:2\(168\)](https://doi.org/10.1061/(ASCE)0733-9445(2001)127:2(168)).